GEOPHYSICAL RESEARCH LETTERS, VOL. 17, NO. 8, PAGES 1049-1052, JULY 1990

FRACTAL BOUNDARIES IN MAGNETOTAIL PARTICLE DYNAMICS

J. Chen, J. L. Rexford*

Space Plasma Branch, Plasma Physics Division, Naval Research Laboratory

Y. C. Lee

University of Maryland and Los Alamos National Laboratory

Abstract. It has been recently established that particle dynamics in the magnetotail geometry can be described as a nonintegrable Hamiltonian system with well-defined entry and exit regions through which stochastic orbits can enter and exit the system after repeatedly crossing the equatorial plane. It is shown that the phase space regions occupied by orbits of different numbers of equatorial crossings or different exit modes are separated by fractal boundaries. The fractal boundaries in an entry region for stochastic orbits are examined and the capacity dimension is determined.

Introduction

Properties of magnetospheric plasmas play an essential role in a wide range of magnetospheric and ionospheric phenomena. One region of importance is the magnetotail where numerous plasma processes can take place, such as instabilities, reconnection, particle acceleration, and particle precipitation into the ionosphere.

As a simple form, the magnetotail magnetic field is often modeled by a magnetic neutral sheet with a superimposed magnetic field component (B_z) normal to the plane (x-y) of the neutral sheet. The nature of charged particle motion in such field configurations has long attracted wide attention (*e.g.*, Speiser, 1965; Sonnerup, 1971; Wagner *et al.*, 1979; Gray and Lee, 1982; Birmingham, 1984; Lyons, 1984; Basu and Rowlands, 1986). It was found (Chen and Palmadesso, 1986; hereafter Paper 1) that such a magnetotail topology is a nonintegrable Hamiltonian system with only two constants of motion in involution, a previously unrealized property. More recently, Chen and Mitchell (1990) have studied a simpler "tri-linear" model in which the particle motion can be reduced to an analytic mapping and which exhibits the essential structures of surfaces of section reported in Paper 1. The chaotic particle motion in the magnetotail has attracted considerable attention in the literature recently (*e.g.*, Büchner and Zelenyi, 1986, 1987, 1989; Chen *et al.*, 1990; Horton and Tajima, 1990). It is interesting that the phase-space structures exhibited by certain chemical reaction dynamics (Skodje and Davis, 1988) are very similar to those described in Paper 1.

*Science Applications International Corporation

Paper number 90GL00709;
0094-8276/90/90GL-00709$03.00

The magnetotail particle motion has well-defined entry and exit regions in the phase space (Paper 1). This is important because the Central Plasma Sheet field lines are finite in length. Particles execute different numbers of equatorial or midplane ($z = 0$) crossings between entry and escape. It has been shown in simple Hamiltonian systems that fractal boundaries can exist with respect to multiple exit modes (Bleher *et al.*, 1988). In this paper, we report the first documentation of fractal boundaries for the particle dynamics in the magnetotail geometry. In particular, we show fractal boundaries with respect to the crossing numbers and exit modes.

Model

The model we use is the modified Harris configuration. The magnetic field is given by

$$\mathbf{B}(x,z) = B_o \tanh(\frac{z}{\delta})\hat{\mathbf{x}} + B_n \hat{\mathbf{z}}, \qquad (1)$$

where B_o and B_n are constant and δ is the half-thickness of the current sheet. The usual magnetospheric coordinate system is used with the x axis in the sun-earth direction. The motion of charged particles is governed by $m d\mathbf{v}/dt = (q/c)\mathbf{v} \times \mathbf{B}$, where m is the mass, q is the electric charge, c is the speed of light and $\mathbf{v} = d\mathbf{x}/dt$ is the particle velocity. Hereafter, q will be taken to be positive. In this paper, we will use the normalized coordinates $X \equiv (x - P_y/m\Omega_n)/(b_n\delta)$, $Y \equiv (y + C_x/m\Omega_n)$, $Z \equiv z/(b_n\delta)$ with $b_n \equiv B_n/B_o$, and $\tau \equiv \Omega_n t$. The normalized velocity is then $\mathbf{V} = d\mathbf{X}/d\tau$. The normalized Hamiltonian is $\hat{H} \equiv H/(mb_n^2\Omega_n^2\delta^2)$. The constants P_y, the canonical momentum, and C_x are associated with y- and x-motion, respectively. However, H, P_y and C_x are not all in involution; $[C_x, P_y] = -m\Omega_n \neq 0$ (Paper 1).

Fractal boundaries

As a concrete example, we have chosen the value $\hat{H} = 500$. Figure 1, adapted from Paper 1, is a Poincare surface of section at $Z = 0$ and shows the entry, stochastic and exit regions. For this value of $\hat{H}$, the stochastic particles have two well-defined entry regions (S1 and T1) and two exit regions, represented by the cross-hatched regions. (See Paper 1 for more detail.) We have chosen orbits in S1 and followed them numerically until their last crossing points (escape points) in the cross-hatched regions. We then classify the initial orbits according to whether they escape from the exit region on the right ($X > 0$) or from the one on the left ($X < 0$). The inital points (the pre-image) can be color-coded according to the exit regions or total number of crossings. Figure 2

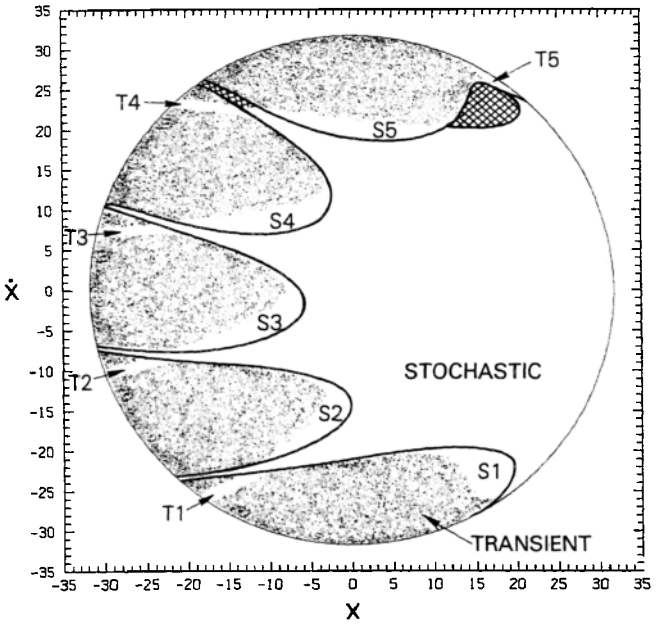

Fig. 1. Phase space structures for the modified Harris field. $\hat{H} = 500$. S1 and T1 are the entry regions and the cross-hatched regions are exit regions for stochastic orbits. Adapted from Paper 1.

shows the fine structure inside S1. The horizontal axis is X and the vertical axis is $\dot{X}$, as in the later figures. The red dots are those initial orbits that escape from the right exit region while the yellow dots are those that escape from the one on the left. The large solid yellow region corresponds to transient orbits and the blue region is in the stochastic region outside S1 (see Fig. 1). These regions are not considered. The boundary at the lower right corner corresponds to the circle in Fig. 1, outside of which orbits are not kinematically allowed. To highlight the basic structure, orbits with more than 20 equatorial crossings are colored black.

Figure 2 shows that the pre-image in S1 on this scale consists of whorl-like striations. Figure 3(a) shows an enlargement of a region of side 10^{-5}. This region is located near $X = 16.5$ and $\dot{X} = -21.5$ where the overall striations are nearly vertical. The red bands are non-fractal, consisting of orbits crossing the equatorial plane a total of 14 times and escaping through the exit region on the right. Hereafter, we will use the notation $n(+)$ to denote orbits which cross the midplane n times and escape from the right ($X > 0$). The notation $n(-)$ refers to escape from the left ($X < 0$) with n crossings. Thus, the red bands will be denoted by 14(+). To the left of each red band is a thin non-fractal yellow band 13(−). To the left of the yellow band is a blue band 14(−). These bands are separated by narrow gaps containing even finer non-fractal bands with higher crossing numbers. The scattered points (green, *etc.*) are unresolved bands of higher crossing numbers to be discussed below.

Figure 3(b) shows an enlargement of a region of side 1.3×10^{-9}. The structures are similar to those shown in Fig. 3(a). However, the corresponding crossing numbers are greater by 5. For example, bands of 19(+) (green)

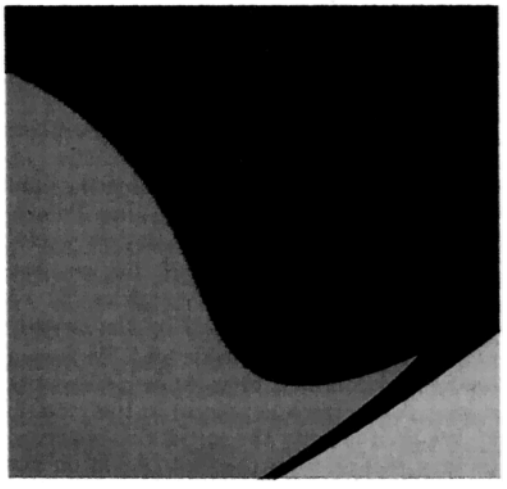

Fig. 2. Pre-image of exit regions in S1. The horizontal axis is X and the vertical axis is $\dot{X}$. The grid is 800×800.

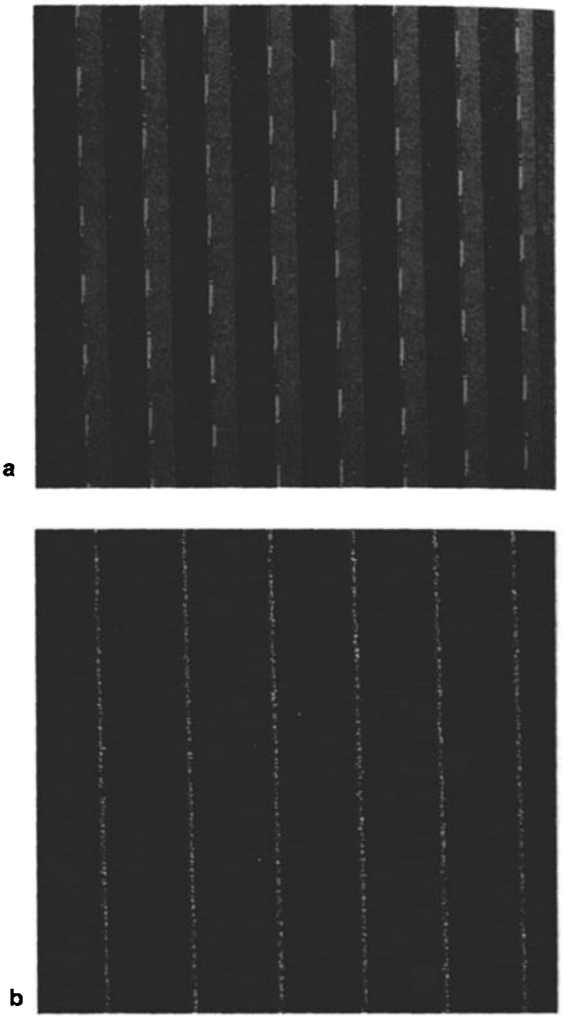

Fig. 3. Enlargement of a small "point" in Fig. 2. The grid is 400×400. Color scheme: grey = 9(+), red=14(+), yellow=13(−), blue=14(−), green= 19(+), white=18(−), and pink=19(−). (a) Each side is 10^{-5}. (b) A square region of sides 1.3×10^{-9}.

correspond to bands of 14(+) (red) and bands of 18(−) (white) correspond to those of 13(−) (yellow). As in Fig. 3(a), the regions between the bands contain unresolved non-fractal bands of higher crossing numbers. Thus, the non-fractal bands are intertwined on finer and finer scales *ad infinitum*. The fuzzy edges of the bands are due to the roundoff errors at this magnification.

There is a specific hierarchy of intertwined non-fractal bands. Figure 3(a) represents the second level of enlargement. The first level consists of bands 9(+) to the right of bands 8(−) and 9(−). Figure 3(a) is on the left edge of a wider (by a few orders of magnitude) band 9(+) and to the right of a band 8(−) (not shown). Figure 3(b) is the third level enlargement. For this example, the minimum number of midplane crossings for stochastic orbits is 8(−). The next larger numbers are 9(+) and 9(−). These orbits traverse the midplane twice before escape (see Paper 1 for more detail on orbits). Each traversal adds five crossings for this example. The pre-images of successive traversals occur on finer scales. Thus, the next traversal leads to the bands 14(+), 13(−) and 14(−) [Fig. 3(a)]. Figure 3(b) corresponds to the next iteration.

Although this example has two exit regions, there are values of $\hat{H}$ with single exit region. The fractal boundaries with respect to the crossing numbers still occur.

The non-fractal bands in Fig. 3 have certain nonlinearity which is not apparent. To determine the nonlinearity, we note that the banded structure is nearly periodic and that the periodicity changes slowly. Such structues can interact with the regular grid to produce characteristic patterns. The plots of Fig. 3 have been made to avoid such "aliasing" effects. Figure 4 shows a square region of side 2×10^{-3} such that the rightmost grey band of Fig. 3(a) corresponds to the rightmost red band 9(+) of Fig. 4. Only those orbits with crossing numbers less than 20 are shown. This figure is on a 400×400 grid and shows prominent arch-like structures consisting of segments of non-fractal bands. All the bands are actually continuous. These arches are nearly periodic both in X and $\dot{X}$. If the bands were straight, no such pattern would emerge. (The fractal nature refers to the "infinitely" intertwined bands and not to the nonlinearity. The arches are related only to the nonlinearity.) In order to understand this pattern, we consider a function $\phi(X, \dot{X})$. A line is then given by $\phi = C(\lambda)$ where C is a constant parametrized by λ. To represent quasi-periodic bands, we consider, as a simple form, $\exp(i\phi)$ or ϕ modulo 2π. Let the grid spacing be Δ. If we expand ϕ about some point, call it, $X = 0$ and $\dot{X} = 0$, then

$$\phi(X, \dot{X}) = \phi_o + a_o X + (1/2) b_o X^2 + c_o \dot{X},$$

with $a_o = (\partial\phi/\partial X)$, $b_o = (\partial^2\phi/\partial X^2)$ and $c_o = (\partial\phi/\partial\dot{X})$. If we write $X = m\Delta$ and $\dot{X} = n\Delta$, it can be shown that an arch is described by $(b_o/2)\Delta^2 \hat{m}^2 + n c_o \Delta =$ constant in the neighborhood of a peak, where $m = m_o + \hat{m}$ with $\hat{m}$ the number of grid points from the peak m_o. The peak of an arch is a parabola. Here, we neglect the small correction if the peak does not fall exactly on a grid point. It can be shown further that the X-distance D_x and the vertical distance D_v between adjacent peaks are

$$D_x = (a_o/b_o) \qquad \text{and} \qquad D_v = 2\pi/c_o. \tag{2}$$

This implies that the "artificial" pattern is a sensitive diagnostic of the nonlinearity of the structure. Both D_x and D_v are independent of the grid spacing Δ. We have enlarged a small region of Fig. 4 by a factor of 5×10^4 and obtained an essentially self-similar pattern (not shown), indicating that the nonlinearity is nearly self-similar and that the non-fractal bands are smooth along the edges. This process of diagnosing the nonlinearity can be likened to the use of diffraction gratings.

We have measured the capacity dimension for a subregion of Fig. 4 using the final-state sensitivity method (Grebogi *et al.*, 1983). (The arch pattern has no bearing on the dimension.) This subregion is a square of sides $\sim 1.5 \times 10^{-3}$ excluding the non-fractal region 9(+) on the right. We choose points randomly within the square and perturb their positions by a small number ϵ. We then calculate the exit modes for each pair to obtain the fraction $f(\epsilon) \equiv N'/N_T$ where N' is the number of pairs whose exit modes are altered as a result of the perturbation and N_T is the total number of pairs used. We have used 2000 to 4000 pairs to obtain N' greater than 100. (N' ranged from ~ 100 to ~ 200.) The statistical uncertainty in $f(\epsilon)$ is $\sim (N')^{-1/2}$ percent. Figure 5 shows $f(\epsilon)$ versus ϵ on a log-log plot. The results are denoted by solid squares with a straight line A to fit them. We have also measured the dimension of a larger area of sides $\sim 6 \times 10^{-2}$. The results are given by solid circles with a straight line B to fit them. From this figure, the uncertainty exponent α is obtained by assuming the scaling relation $f(\epsilon) \sim \epsilon^{\alpha}$. Our fit gives $\alpha \simeq 0.22$ for both A and B, giving the dimension of $d = 1 - \alpha \simeq 1.8$. For different cutoff numbers less than 50, we have found nearly the same values for α.

We have repeated the same procedure with no cutoff in the crossing numbers. The resulting $f(\epsilon)$ is shown by open squares and circles, corresponding to the solid squares and circles, respectively. We find that α decreases slightly as ϵ is made smaller. The orbits with large crossing numbers (the highest found was 6979) execute many crossings just outside the outermost Kolmogorov-Arnol'd-Moser (KAM) surface, which has complicated small-scale structures (Greene, 1979) leading to "stickiness". We believe that this stickiness is responsible for

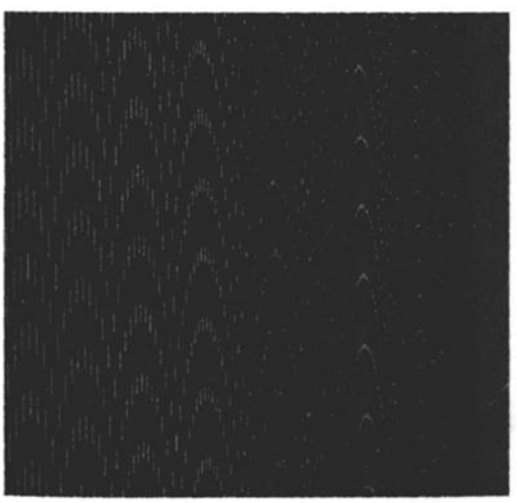

Fig. 4. Interference between the regular grid and nonlinearity of the non-fractal bands (Fig. 3). Red: escape from the right. Yellow: escape from the left. Crossing numbers are not distinguished. The arches are spaced by D_x horizontally and D_v vertically [eq. (2)].

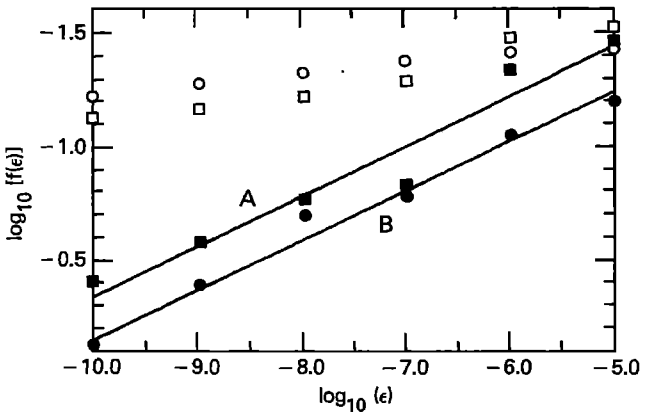

Fig. 5. $f(\epsilon)$ versus ϵ plotted on a log-log scale. Solid squares are obtained from a subregion of Fig. 4 (line A) and solid circles are obtained from a larger region (line B). Open squares and circles denote results with no cutoff in the total crossing numbers for the respective regions.

the decreasing α. Bleher *et al.* (1988) encountered a similar effect when they plotted $f(\epsilon)$ for trapped orbits. They attributed this to the stickiness of the boundary of trapped orbits.

Discussion

In this paper, we have provided for the first time numerical evidence of fractal boundaries for particle dynamics in the magnetotail topology. One value $\hat{H} = 500$ has been used as an example. We have also determined the capacity dimension to be approximately $d \simeq 1.8$ for the region examined. We expect that the essential conclusions of this paper are applicable to other values of $\hat{H}$ and other similar systems.

A number of potentially important effects of stochastic particle motion have been considered. Paper 1 suggested that the process of "differential memory" would generate non-Maxwellian free-energy in a dynamic environment. This process has been verified recently (Chen *et al.*, 1990). Büchner and Zelenyi (1987) suggested that chaotic electron orbits could destabilize the collisionless tearing mode. Horton and Tajima (1990) have considered the "collisionless conductivity" including stochastic orbits. It is thus important to understand the nature of this dynamical system. It has been suggested by Büchner and Zelenyi (1989) that the crossing of separatrix in the effective potential is the essential mechanism for chaos. In contrast, Chen and Mitchell (1990) have used an analytical "tri-linear" model to show that a stretch-and-fold mapping associated with the gyration and reflection of orbits produces the essential phase space structures reported in Paper 1. This mapping is shown to produce fractal boundaries similar to those described in this paper. The fractal boundaries constitute a specific property which a proposed mapping should produce. Furthermore, viewed as a chaotic scattering mechanism, the fractal boundaries affect relationships between the destribution of incoming orbits (*e.g.*, of ionospheric origin) and that of the outgoing orbits, *i.e.*, the final states.

Acknowledgments. We wish to thank Dr. G. Burkhart for his help in computing orbits and Dr. E. Ott for useful discussions. This research was supported by NASA (W-16991) and the Office of Naval Research.

References

Basu, S. and G. Rowlands, Analytical treatment of charged particle motion in the geomagnetotail, *Planet. Space Sci., 34*, 631, 1986.

Birmingham, T. J., Pitch angle diffusion in the Jovian magnetodisc, *J. Geophys. Res., 89*, 2699, 1984.

Bleher, S., C. Grebogi, E. Ott, and R. Brown, Fractal boundaries for exit in Hamiltonian dynamics, *Phys. Rev. A, 38*, 930, 1988.

Büchner, J. and L. M. Zelenyi, Deterministic chaos in the dynamics of charged particles near a magnetic field reversal, *Phys. Lett. A. 118*, 395, 1986.

Büchner, J. and L. M. Zelenyi, Chaotization of the electron motion as the cause of an internal magnetotail instability and substorm onset, *J. Geophys. Res., 92*, 13456, 1987.

Büchner, J. and L. M. Zelenyi, Regular and chaotic motion in tail-like magnetic field reversal 1. Basic theory of trapped motion, *J. Geophys. Res., 94*, 11821, 1989.

Chen, J. and H. G. Mitchell, Stochastic particle dynamics in the magnetotail, in preparation, 1990.

Chen, J., H. G. Mitchell and P. J. Palmadesso, Differential memory in the tri-linear model magnetotail, in press, *J. Geophys. Res.*, 1990.

Chen, J. and P. J. Palmadesso, Chaos and nonlinear dynamics of single-particle orbits in a magnetotaillike magnetic field, *J. Geophys. Res., 91*, 1499, 1986.

Gray, P. and L. C. Lee, Particle pitch angle diffusion due to nonadiabatic effects in the plasma sheet, *J. Geophys. Res., 87*, 7445, 1982.

Grebogi, C., S. W. McDonald, E. Ott, and J. A. Yorke, Final state sensitivity: an obstruction to predictability, *Phys. Lett., 99A*, 415, 1983.

Greene, J. M., A method for determining a stochastic transition, *J. Math. Phys., 20*, 1183, 1979.

Horton, W. and T. Tajima, Decay of correlations and the collisionless conductivity in the geomagnetic tail, in press, *Geophys. Res. Lett.*, 1990.

Lyons, L. R., Electron energization in the geomagnetic tail current sheet, *J. Geophys. Res., 89*, 5479, 1984.

Skodje, R. T. and M. J. Davis, A phase space analysis of the collinear I+HI reaction, *J. Chem. Phys., 88*, 2429, 1988.

Sonnerup, B. U. Ö., Adiabatic particle orbits in a magnetic null sheet, *J. Geophys. Res., 76*, 8211, 1971.

Speiser, T. W., Particle trajectories in model current sheets, 1, Analytical solutions, *J. Geophys. Res., 70*, 4219, 1965.

Wagner, J. S., J. R. Kan, and S.-I. Akasofu, Particle dynamics in the plasma sheet, *J. Geophys. Res., 84*, 891, 1979.

J. Chen, Code 4781, Naval Research Laboratory, Washington, DC 20375-5000.

Y. C. Lee, Laboratory for Plasma Research, University of Maryland, College Park, MD 20742.

J. L. Rexford, Science Applications International Corp. McLean, VA 22102.

(Received November 10, 1989;
revised March 19, 1990;
accepted March 19, 1990)